PCCP

Accepted Manuscript

ROYAL SOCIETY OF CHEMISTRY

www.rsc.org/pccp

Synthesis and decomposition of $Li_3Na(NH_2)_4$ and investigations of Li–Na–N–H based systems for hydrogen storage

Lars H. Jepsen[a], Peikun Wang[b], Guotao Wu[b], Zhitao Xiong[b], Flemming Besenbacher[c], Ping Chen[b*]

and Torben R. Jensen[a*]

[a]*Center for Materials Crystallography, Interdisciplinary Nanoscience Center and Department of Chemistry, Aarhus University, Langelandsgade 140, 8000 Aarhus C, Denmark*

[b]*Dalian Institute of Chemical Physics, Chinese Academy of Sciences,116023, P.R. China*

[c]*Interdisciplinary Nanoscience Center (iNANO) and Department of Physics and Astronomy, Aarhus University, Ny Munkegade 120, DK-8000 Aarhus C, Denmark.*

*Corresponding authors

Abstract

Previous studies have shown modified thermodynamics of amide-hydride composites by cation substitution, while this work systematically investigates lithium-sodium-amide, Li–Na–N–H, based systems. $Li_3Na(NH_2)_4$ has been synthesized by combined ball milling and annealing of $3LiNH_2$–$NaNH_2$ with $LiNa_2(NH_2)_3$ as a minor by-product. $Li_3Na(NH_2)_4$ releases $NaNH_2$ and forms non-stoichiometric $Li_{3+x}Na_{1-x}(NH_2)_4$ before it melts at 234 °C, as observed by *in-situ* powder X-ray diffraction. Above 234 °C, $Li_{3+x}Na_{1-x}(NH_2)_4$ releases a mixtures of NH_3, N_2 and H_2 while a bi-metallic lithium sodium imide is not observed during decomposition. Hydrogen storage performances have been investigated for the composites $Li_3Na(NH_2)_4$–$4LiH$, $LiNH_2$–NaH and $NaNH_2$–LiH. $Li_3Na(NH_2)_4$–$4LiH$ converts into $4LiNH_2$–NaH–$3LiH$ during mechanochemical treatment and releases 4.2 wt% of H_2 in multiple steps between 25 and 340 °C revealed by Sievert's measurements. All three investigated composites have a lower peak temperature for H_2 release as compared to $LiNH_2$-LiH, possible owing to modified kinetics and thermodynamics, due to the formation of $Li_3Na(NH_2)_4$ and $LiNa_2(NH_2)_3$.

Table of Content Figure

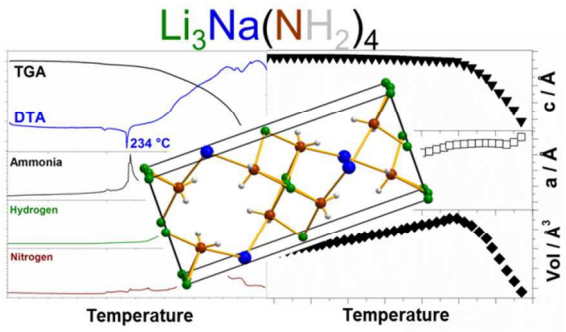

$Li_3Na(NH_2)_4$ melts at 234 °C and improves the kinetics for H_2 release from Li-Na-N-H based composites.

Keywords: Metal amides, $Li_3Na(NH_2)_4$, $LiNa_2(NH_2)_3$, hydrogen storage,

1. Introduction

Discovery of a safe and efficient way to store hydrogen is among the most challenging tasks in the transition to a hydrogen-based society. Solid-state storage may provide high hydrogen capacities both gravimetrically and volumetrically,[1,2] and a promising candidate is Li_3N, which reversibly stores 10.4 wt% H_2 in two steps according to the reaction scheme (1).[3]

$$Li_3N(s) + 2H_2(g) \leftrightarrow Li_2NH(s) + LiH(s) + H_2(g) \leftrightarrow LiNH_2(s) + 2LiH(s) \quad (1)$$

However, only the second step (*i.e.* the imide-amide transition) is reversible under practical conditions, although the enthalpy of reaction is still relatively high (ΔH = 66 kJ/mol),[4,5] leading to an operating temperature at ~280 °C under $p(H_2)$ = 1 bar. Efforts have been devoted to destabilization of the Li–N–H system by replacing lithium amide with other amides in composites such as $Mg(NH_2)_2$–LiH,[6–8] or substitution of LiH by $LiAlH_4$, *i.e.* $LiAlH_4$–$LiNH_2$.[9,10] Composites based on Li–Na–N–H, *e.g.* $LiNH_2$–NaH or $NaNH_2$–LiH, are not described in the literature, possibly because sodium imide remains unknown, and only few hydrogen storage systems based on $NaNH_2$ have been investigated.[11–16] Recently, $NaNH_2$ and Li_2NH were used as cheap and efficient catalysts for the cracking of NH_3 into H_2 and N_2.[17–19] $NaNH_2$ melts at ~200 °C and is reported to decompose into the elements, although the decomposition remains not fully understood.

To our knowledge, the only reported bi-metallic amides investigated for hydrogen storage are $LiAl(NH_2)_4$–LiH (1:4),[20] $Li_4[Zn(NH_2)_4](NH_2)_2$–LiH (1:12) and $K_2[Zn(NH_2)_4]$–LiH (1:8),[21] whereby the latter mixture can be fully hydrogenated within 30 s at 230 °C. The bi-metallic amides $LiNa_2(NH_2)_3$, $Li_3Na(NH_2)_4$ and $Li_5Na(NH_2)_6$ were first reported in 1982,[22] and more recently solid solutions were observed for $Li_{3+x}Na_{1-x}(NH_2)_4$ ($0 \leq x \leq 1.0$).[23] However, due to the lack of phase pure samples of $LiNa_2(NH_2)_3$ and $Li_3Na(NH_2)_4$, the thermal decomposition mechanism remains unknown.

We report the synthesis and thermal decomposition of $Li_3Na(NH_2)_4$, and the mixtures of $Li_3Na(NH_2)_4$–4LiH, $LiNH_2$-NaH and $NaNH_2$-LiH are systematically investigated as potential hydrogen storage composites.

2. Experimental

2.1 Sample preparation

$LiNH_2$ (95%, Aldrich), $NaNH_2$ (98%, Aldrich), LiH (98%, Aldrich), and NaH (95%, Aldrich) were used as received. Powder X-ray diffraction data reveal that both NaH and $NaNH_2$ contain small amounts of impurities of NaOH. All sample handling were performed in an argon-filled MBraun glovebox with O_2 and H_2O concentrations < 1 ppm. An overview of all samples including synthesis procedures is provided in Table 1.

$Li_3Na(NH_2)_4$ was synthesized by ball milling mixtures of $LiNH_2$–$NaNH_2$ (3:1) for 5 min (s1), 20 min (s2) and 90 min (s3), respectively, using a high energy Spex ball mill. Subsequently, s3 was annealed at 150 °C for 6 h (s4). In order to eliminate the potential catalyzing effect of contaminations of stainless steel from the ball milling jars, $Li_3Na(NH_2)_4$ was also prepared by ball milling $LiNH_2$–$NaNH_2$ (3:1) for 20 h at a Retsch PM400 planetary ball mill using agate (SiO_2) jars before annealing at 150 °C (s5).

The samples $Li_3Na(NH_2)_4$–LiH (1:4, s8), $LiNH_2$–LiH (1:1, s9), $LiNH_2$–NaH (1:1, s10), $NaNH_2$–LiH (1:1, s11) and $LiNH_2$ (s12) were loaded in stainless steel vials and stainless steel balls with ball to powder mass ratio 40:1. Subsequently, ball milling was carried out using a Retsch PM400 planetary ball mill at 200 rpm for 2 min followed by 15 s break, and this sequence was repeated, giving efficient ball milling times at 10 h. The pressures in the ball milling vials were carefully monitored for all samples, revealing that no gasses were released during ball milling. Additionally, $Li_3Na(NH_2)_4$–LiH (1:4) was ball milled using the same setup, but only for 1.5 h (s7), and $Li_3Na(NH_2)_4$–LiH (1:4) was manually grinded for 5 min using a mortar (s6). Fractions of $LiNH_2$–NaH (1:1, s10) were heated to 110, 185 and 270 °C, respectively, in a stainless steel reactor in inert atmosphere and subsequently cooled to RT. These samples are denoted s10_110, s10_185, s10_270, respectively.

2.2 Sample characterization

Laboratory powder X-ray diffraction (PXD). Powder X-ray diffraction (PXD) measurements were conducted to identify crystalline products with a PANalytical X'pert diffractometer, Cu Kα1 radiation, $\lambda = 1.54060$ Å.

Synchrotron radiation powder X-ray diffraction (SR-PXD). *In-situ* SR-PXD data were measured for $Li_3Na(NH_2)_4$ (s4) at beamline I711 at the MAX-II synchrotron in the research laboratory MAX-lab, Lund, Sweden with a MAR165 CCD detector system and a selected wavelength of $\lambda = 0.99203$ Å. The sample was mounted in a sapphire (Al_2O_3) single-crystal tube (1.09 mm o.d., 0.79 mm i.d.) in an argon filled glovebox ($p(O_2, H_2O) < 0.5$ ppm), using a specially designed sample holder.[24] The *in-situ* SR-PXD data were conducted from RT to 500 °C (5 °C/min) in argon atmosphere. Additionally, SR-PXD data were measured for $Li_3Na(NH_2)_4$ (s4) at the Swiss-Norwegian Beamline at ESRF, Grenoble, France, with a Pilatus 2M detector, where the powder was loaded in a 0.5 mm glass capillary. All obtained raw images were transformed to 2D-powder diffraction patterns using the FIT2D program,[25] which was also used to remove diffraction spots from the single-crystal sapphire tube used as sample holder. The intensities of selected Bragg diffraction peaks were fitted to a Gaussian curve for each diffraction pattern. Subsequently, the integrated reflections were plotted in order to illustrate changes in the sample composition as a function of temperature. Rietveld refinements were performed using the Fullprof program.[26]

Thermogravimetric analysis and differential thermal analysis. Simultaneous thermogravimetric analysis (TGA) and differential thermal analysis (DTA) were conducted on a Netsch 449C TG/DSC. The samples (approx. 5 mg) were heated from RT to 550 °C with a heating rate of 2 °C/min in an Al_2O_3 crucible with a small Al_2O_3 lid. The Netsch 449C apparatus was placed inside a MBraun argon filled glovebox and purified argon was employed as a carrier gas during the measurements.

Calorimetric measurements. A C80 Setaram was used for closed-system calorimetric measurements. Samples (approx. 100 mg) were loaded in a closed stainless steel reactor and heated from RT to 220 °C with a heating rate of 0.5 °C/min.

Temperature-programmed desorption mass spectroscopy (TPD-MS). The thermal desorption behavior of all samples were studied using a homemade temperature programmed desorption (TPD) setup connected to a mass spectrometer (MS, Hiden HPR-20) to identify the gaseous products. Purified argon was used as a carrier gas and all samples were studied from 30 to 500 °C with a heating rate of 2 °C/min. The samples were loaded in a stainless steel reactor, which may catalyze decomposition of released NH_3 into N_2 and H_2 above 300 °C.

Sievert's measurements. Sieverts measurements were performed using a PCTPro-2000 apparatus in order to determine the amount of released hydrogen. Samples (approx. 100 mg) were heated with 1 °C/min under static vacuum in a stainless steel reactor.

Fourier transform infrared spectroscopy (FTIR). Fourier transform infrared spectroscopy (FTIR) measurements were conducted on a Varian 3100 unit in DRIFT mode under argon atmosphere. The samples were exposed to the IR light for 32 s for each experiment.

Determination of NH_3 concentration. The concentration of NH_3 released during thermal decomposition were determined quantitatively by using a conductivity meter (Thermo Scientific) with an accuracy of 0.1 μS/cm. Samples were heated from 30 to 500 °C (2 °C/min) using the TPD-setup and the released gasses were carried by an argon flow to the conductivity cell, which was filled with diluted H_2SO_4 (0.006 M). From the linear relationship between NH_3 and the decrease in conductivity, the amount of NH_3 was calculated.

Temperature-programmed photographic analysis (TPPA) Approx. 10 mg of the samples were sealed under argon in a glass tube placed in a home-built aluminum heating block as described recently.[27] The samples were heated from RT to 450 °C (heating rate 5 °C/min), while photos of the sample were collected every five second.

3. Results and Discussion

3.1 Synthesis and thermal decomposition of $Li_3Na(NH_2)_4$.

The mixture of $LiNH_2$–$NaNH_2$ (3:1) was ball milled for various times using a high energy ball mill. PXD data (Figure 1) after 5 min ball milling (s1) reveal Bragg reflections from $NaNH_2$, $LiNH_2$, $LiNa_2(NH_2)_3$ and weak peaks from $Li_3Na(NH_2)_4$; PXD data after 20 min ball milling (s2) show $LiNH_2$, $LiNa_2(NH_2)_3$ and $Li_3Na(NH_2)_4$, while after 90 min ball milling (s3) reflections are only observed from $Li_3Na(NH_2)_4$ and minor reflections from $LiNa_2(NH_2)_3$, according to reaction scheme (2). Higher purity of $NaNH_2$ (98%) than $LiNH_2$ (95%) was used in the synthesis, which may lead to the formation of $LiNa_2(NH_2)_3$.

$$6LiNH_2(s) + 2NaNH_2(s) \rightarrow LiNa_2(NH_2)_3(s) + 5LiNH_2(s) \rightarrow 2Li_3Na(NH_2)_4(s) \quad (2)$$

In order to complete reaction (2), s3 was annealed at 150 °C for 6 h (s4), below the onset temperature for gas release for s3, 160 °C. Rietveld refinement of SR-PXD data collected at RT (Figure S1) reveal that s4 consists of $Li_3Na(NH_2)_4$ (94 wt%) with small amounts of $LiNa_2(NH_2)_3$ (6 wt%). FTIR spectra (Figure S2) confirm that weak N-H bands from $LiNH_2$ observed for s3 have disappeared after annealing, while the two N-H stretches from $Li_3Na(NH_2)_4$ are identified at 3294 and 3238 cm^{-1} in accord with the literature.[11] The purity of $Li_3Na(NH_2)_4$ (94 wt%) in this sample is slightly higher than what was obtained in the literature (90 wt%) from a hand ground mixture of $LiNH_2$–$NaNH_2$ (3:1) annealed at 200 °C for 12 h.[23] This may arise from the fact that less pure $NaNH_2$ (90 %) was used in the previous work.

The fast formation of $LiNa_2(NH_2)_3$ (within 5 min of ball milling) suggests that the activation energy may be lower for the formation of $LiNa_2(NH_2)_3$ than for $Li_3Na(NH_2)_4$. $LiNH_2$ is initially dissolved in $NaNH_2$, which may be a faster reaction as compared to $LiNH_2$ dissolved in $LiNa_2(NH_2)_3$. The unit cell volume of $Li_3Na(NH_2)_4$ is ~3 % larger than the sum of the volumes of $3LiNH_2$ and $NaNH_2$, while $LiNa_2(NH_2)_3$ is ~13 % smaller than the sum of the volumes of $LiNH_2$ and $2NaNH_2$. This may also explain why $LiNa_2(NH_2)_3$ is readily formed by mechanochemical treatment, *i.e.* compression, and $Li_3Na(NH_2)_4$ is produced upon prolonged mechanochemical and heat treatment, *i.e*. thermal expansion.

$Li_3Na(NH_2)_4$ crystallizes in a tetragonal unit cell with space group symmetry *I*-4 similar to $LiNH_2$ and has also a similar unit cell volume as $LiNH_2$.[22,23] Hence, $Li_3Na(NH_2)_4$ can be considered as an ordered variant of $LiNH_2$ with Li^+ substituted by Na^+ at the 2*c* site. All Li^+ and Na^+ atoms are tetrahedrally coordinated by NH_2^-. In contrast, 3/4 of the Na^+ cations in $LiNa_2(NH_2)_3$ (space group $P4_2/m$) are positioned at the 2*a* and 4*i* sites with octahedral coordination and ¼ of the Na^+ cations at the 2*f* site with tetrahedral coordination.[22,23] Recent theoretical studies of high-pressure polymorphs of $NaNH_2$ suggest that the octahedral coordination of Na^+ atoms are less stable and have higher energies compared to the tetrahedral coordination,[28] suggesting that the formation of $Li_3Na(NH_2)_4$ is more thermodynamically favorable than that of $LiNa_2(NH_2)_3$, in accord with scheme (2). This contrast ref[23] suggesting that $LiNa_2(NH_2)_3$ is more thermodynamically stable than $Li_3Na(NH_2)_4$.

The thermal decomposition of $Li_3Na(NH_2)_4$ (s4) was characterized by TGA/DTA and TPD-MS (Figure 2) from RT to 475 °C (2 °C/min). The DTA reveals a small endothermic event at 196 °C and a major event at 234 °C, the latter being due to the melting of $Li_3Na(NH_2)_4$, as determined by TPPA (Figure S3). The latent heat of fusion for $Li_3Na(NH_2)_4$ was determined to 11.3 kJ/mol by calorimetric measurements conducted in a closed vessel (Figure S4). TGA data (Figure 2) reveal a total mass loss of ~45 wt% up to 475 °C, while TPD-MS reveals that a mixture of NH_3, N_2 and H_2 is released. The amount of NH_3 released from RT to 500 °C was quantified to 1.7 mol of NH_3 per mol $Li_3Na(NH_2)_4$ (Figure S5). Noteworthy, ~84 mol% of the NH_3 is released before 300 °C, while $LiNH_2$ ball milled for 10 h (s13) has only released ~14 mol% NH_3 at 300 °C (Figure S6). Thus, $Li_3Na(NH_2)_4$ is less stable and/or shows faster kinetics for the decomposition than $LiNH_2$, which can be explained by the lower melting point for $Li_3Na(NH_2)_4$ (234 °C) compared to $LiNH_2$ (370 °C).[29] $KLi_3(NH_2)_4$ releases also NH_3 at a significantly lower temperature than $LiNH_2$ with an onset temperature below 100 °C.[30] Traces of steel from the ball milling process may catalyze the decomposition of $Li_3Na(NH_2)_4$. Therefore, a sample of $Li_3Na(NH_2)_4$ (denoted s5) was synthesized by using agate vials rather than stainless steel vials. However, the thermal analysis for s4 and s5 are identical.

In-situ SR-PXD data were obtained for $Li_3Na(NH_2)_4$ (s4) from RT to 440 °C (5 °C/min), Figure 3. At RT, Bragg reflections are present from $Li_3Na(NH_2)_4$ and trace amounts of $LiNa_2(NH_2)_3$ and Li_2O. During heating, the weak reflections from $LiNa_2(NH_2)_3$ disappear at 200 °C and no new peaks appear (Figure 3b). The reflections from $Li_3Na(NH_2)_4$ slowly decrease in intensity at $T > 50$ °C and faster at 200 °C, and disappear at 230 °C, where relatively weak reflections from $LiNH_2$ appear. At 320 °C, $LiNH_2$ disappears and no new reflections appear before the experiment was stopped at 440 °C, where only weak reflections from Li_2O are observed. The expected formation of Li_2NH may not be observed due to melting of $LiNH_2$ that causes the solid material to float out of the volume exposed to the X-ray beam. A noteworthy change in the unit cell dimensions of the tetragonal $Li_3Na(NH_2)_4$ is observed by sequential Rietveld refinement (Figure 4). From RT to 200 °C, approx. linear thermal expansion is observed in the *a*,*b*-directions, while the *c* parameter remains constant up to 200 °C. The linear thermal expansion coefficients were calculated for $\alpha_{a,b} = 5.62 \cdot 10^{-4}$ K^{-1} (T = 23-180 °C) and $\alpha_V = 1.11 \cdot 10^{-4}$ K^{-1} (T = 23-180 °C). From 200 to 230 °C, a remarkable decrease in *c* is observed, while *a*,*b* stay constant, which may be due to the formation of non-stoichiometric $Li_{3+x}Na_{1-x}(NH_2)_4$, as reported in the

literature.[23] In other words, $NaNH_2$ is released from the $Li_3Na(NH_2)_4$ structure prior to the melting. It is reported that the unit cell volume for $Li_{3+x}Na_{1-x}(NH_2)_4$ decrease for increasing x.[23] However, both a and c are reported to decrease with increasing x in contrast to the data presented here. Similar to the c-axis in $Li_3Na(NH_2)_4$, the lattice parameter b in the structure of $NaSc(BH_4)_4$ shows a significant anomaly close to the melting temperature.[31]

An *ex-situ* investigation of $Li_3Na(NH_2)_4$ heated to 450 °C reveals Bragg reflections from Li_2NH according to PXD measured at RT. Additionally, the surface of the reactor was covered by a soft and shiny metal, assigned to sodium. A bi-metallic lithium sodium nitride or imide (*e.g.* $Li_3Na(NH)_2$) is not observed during the thermal decomposition. The formation of nitrides or imides is required in order to obtain a reversible hydrogen storage system, *e.g.* the $Mg(NH_2)_2$–2LiH mixture produces $Li_2Mg(NH)_2$ upon thermal treatment.[32]

3.2 Composites of $Li_3Na(NH_2)_4$–LiH (1:4)

Samples of $Li_3Na(NH_2)_4$–LiH (1:4) were prepared, in attempts to obtain enhanced kinetics compared to the $LiNH_2$-LiH composite. Samples of $Li_3Na(NH_2)_4$–LiH (1:4) were manually ground for 5 min (s6) or ball milled for 1.5 h (s7) or 10 h (s8). PXD data (Figure 5) and FTIR spectra (Figure S7) reveal that after 10 h of ball milling, $Li_3Na(NH_2)_4$–LiH (1:4) has converted into $LiNH_2$, NaH and LiH according to reaction scheme (3), and therefore ball milled $Li_3Na(NH_2)_4$–LiH (s8) contains $LiNH_2$, NaH and LiH (4:1:3). Similarly, the bi-metallic amide based composites $LiAl(NH_2)_4$–LiH (1:4) and $Li_4Zn(NH_2)_6$–LiH (1:12) were also reported to react during ball milling,[20,21] although the exact reaction mechanisms remain unknown.

$$Li_3Na(NH_2)_4(s) + LiH(s) \rightarrow 4LiNH_2(s) + NaH(s) \quad (3)$$

TPD-MS data were measured for ball milled $Li_3Na(NH_2)_4$–LiH (1:4, s8, Figure 5a) and compared with $LiNH_2$–LiH (s9, Figure 5b) from RT to 475 °C (2 °C/min). $LiNH_2$-LiH (s9) releases H_2 in accord with the literature[4] with a maximum at 242 °C. In contrast, ball milled $Li_3Na(NH_2)_4$–LiH (1:4) releases hydrogen in multiple steps with the main peak for H_2 release at 216 °C and additionally peaks at 296, 316 and 392 °C, respectively. Hence, the main peak temperature for H_2 release at 216 °C is lowered

slightly as compared to $LiNH_2$–LiH (242 °C). Sievert's measurements of ball milled $Li_3Na(NH_2)_4$–LiH (1:4) between RT and 340 °C (Figure S8) reveal that three mol of H_2 are released, corresponding to 4.2 wt% H_2. PXD data of the sample after the Sievert´s measurement contain Bragg reflections from Li_2NH, NaH, $LiNH_2$ and weak reflections from $Li_3Na(NH_2)_4$ and Li_2O (Figure S9). These results prompted further investigations of the simpler composite of $LiNH_2$–NaH.

3.3 Composites of $LiNH_2$–NaH and $NaNH_2$–LiH

A composite of $LiNH_2$–NaH was ball milled for 10 h (s10) and a physical mixture of the starting reactants was obtained, according to PXD (Figure 7) and FTIR (Figure 8a). The thermal decomposition was studied by TPD-MS from RT to 475 °C (2 °C/min, Figure 6c). $LiNH_2$–NaH releases H_2 only below 275 °C with a maximum H_2 release at T_{max} = 232 °C, while a mixture of H_2, N_2 and NH_3 is detected above 275 °C. The H_2 release profile for $LiNH_2$–NaH has previously been reported,[33] and it was speculated that Na_2NH is formed, however, without further experimental investigations. Therefore, *ex-situ* PXD and FTIR measurements were conducted in this project for $LiNH_2$–NaH heated to 110, 185 and 270 °C (denoted s10_110, s10_185 and s10_270, respectively) shown in Figures 7 and 8a. The FTIR spectrum for s10_110 shows weak N-H bands from $Li_3Na(NH_2)_4$, but no diffraction peaks from $Li_3Na(NH_2)_4$ are observed by PXD. However, $Li_3Na(NH_2)_4$ is clearly observed from both PXD and FTIR for s10_185, suggesting that the metathesis reaction (4) takes place. In fact, this is the reverse reaction of reaction scheme (3), which takes place during ball milling of $Li_3Na(NH_2)_4$–LiH (1:4). In accord, '4$LiNH_2$ and LiH' has ~4 % smaller unit cell volume than '$Li_3Na(NH_2)_4$ and LiH' and the formation is therefore favored by compression (scheme 3), while the formation of '$Li_3Na(NH_2)_4$ and LiH' is possibly driven by thermal expansion during heating (scheme 4).

$$4LiNH_2(s) + NaH(s) \rightarrow Li_3Na(NH_2)_4(s) + LiH(s) \quad (4)$$

Sievert's measurements (Figure S10) show that ~0.25 mol of H_2 (~1.0 wt% H_2) are released per $LiNH_2$ up to 270 °C, and PXD and FTIR data for s10_270 reveal the presence of Li_2NH, NaH, $Li_3Na(NH_2)_4$ and $LiNa_2(NH_2)_3$ (Figure 7 and 8). Thus, the reaction for hydrogen release below 270 °C may be described by reaction scheme (5).

$$20LiNH_2(s) + 5NaH(s) \rightarrow 5Li_2NH(s) + 5H_2(g) + 3Li_3Na(NH_2)_4(s) + LiNa_2(NH_2)_3(s) \quad (5)$$

Remaining NaH is observed in the sample at 270 °C because the ratio between $LiNH_2$ and NaH is 1:1 for s10, whereas they react in the ratio 4:1 according to reaction scheme (5). The ratio between the starting reactants was therefore modified to $LiNH_2$–NaH (4:1), however, due to the instability of $LiNa_2(NH_2)_3$ and $Li_3Na(NH_2)_4$ and the absence of excess of NaH to react with the released NH_3, significant amounts of NH_3 are released above 250 °C (Figure S11).

Li–Na–N–H composites starting from $NaNH_2$–LiH were also investigated. PXD and FTIR data (Figures S12 and S13) of $NaNH_2$–LiH after 10 h ball milling (s11) reveal the presence of $Li_3Na(NH_2)_4$ and NaH. Thus, reaction (6) takes place during mechanochemical treatment, and the composition of s11 is $Li_3Na(NH_2)_4$–LiH–NaH in the ratio 1:1:3. Upon prolonged ball milling (72 h) of $NaNH_2$–LiH, no transformation into $LiNH_2$–NaH occurs.

$$4NaNH_2(s) + 3LiH(s) \rightarrow Li_3Na(NH_2)_4(s) + 3NaH(s) \quad (6)$$

Thermal decomposition of ball milled $NaNH_2$–LiH (s11) gives rise to a similar hydrogen profile as observed for $LiNH_2$–NaH (s10, Figure S14), and the same amount of H_2 is released according to Sievert's measurements (Figure S10). PXD and FTIR data for s11_250 (Figures S12 and S13) reveal the presence of NaH, Li_2NH, $Li_3Na(NH_2)_4$ and $LiNa_2(NH_2)_3$; hence, the reaction may occur similarly to the reaction of $LiNH_2$–NaH.

In summary, $Li_3Na(NH_2)_4$ and $LiNa_2(NH_2)_3$ are formed as intermediates during decomposition of $LiNH_2$–NaH which may lower the hydrogen release temperature slightly as compared to $LiNH_2$-LiH, owing to lower thermal stability and lower melting points as compared to $LiNH_2$ (~370 °C). $Li_3Na(NH_2)_4$ and $LiNa_2(NH_2)_3$ can subsequently react with LiH above ~250 °C and release H_2, hence, ball milled $Li_3Na(NH_2)_4$–4LiH releases hydrogen in multiple steps.

Conclusion

Systematic studies of substitution of Na into the well-known $LiNH_2$-LiH composite are presented for the first time. The bi-metallic amide $Li_3Na(NH_2)_4$ has been synthesized by mechanochemical treatment

and annealing of $LiNH_2$–$NaNH_2$ (3:1), and the melting point of $Li_3Na(NH_2)_4$ has been determined to 234 °C. Prior to the melting, $NaNH_2$ is released and the formation of non-stoichiometric $Li_{3+x}Na_{1-x}(NH_2)_4$ is revealed by *in-situ* SR-PXD. The presence of $Li_3Na(NH_2)_4$ and $LiNa_2(NH_2)_3$ during the decomposition of the investigated composites, $Li_3Na(NH_2)_4$–4LiH, $LiNH_2$–NaH and $NaNH_2$–LiH, gives rise to lower temperatures for H_2 release, possible due to lower thermal stability and faster kinetics as compared to $LiNH_2$-LiH. However, in order to have a reversible hydrogen storage system based on metal amides, the formation of metal imides or nitrides is required as seen for $LiNH_2$–LiH and $Mg(NH_2)_2$–2LiH. Hence, the Li–Na–N–H systems are considered non-reversible, because no sodium based compounds in the present work absorbs hydrogen.

Acknowledgement

The Innovation Fund Denmark is acknowledged for financial support to the project HyFillFast, and the Carlsberg Foundation is acknowledged. The Danish National Research Foundation is thanked for funding to the Center for Materials Crystallography (CMC, DNRF93), and the Sino-Danish Center for Education and Research (SDC) is acknowledged. Projects of National Natural Science Foundation of China (Grant nos 51225206, 21273229, U1232120) are also acknowledged. We are also grateful to the Swiss-Norwegian Beamline at ESRF, Grenoble, France and the beam line I711 at MAXlab, Lund, Sweden for the provision of beam time.

References

1 L. H. Jepsen, M. B. Ley, Y.-S. Lee, Y. W. Cho, M. Dornheim, J. O. Jensen, Y. Filinchuk, J. E. Jørgensen, F. Besenbacher and T. R. Jensen, *Materials Today*, 2014, **17**, 129–135.
2 S. I. Orimo, Y. Nakamori, J. R. Eliseo, A. Züttel and C. M. Jensen, *Chem. Rev.*, 2007, **107**, 4111–4132.
3 P. Chen, Z. Xiong, J. Luo, J. Lin and K. L. Tan, *Nature*, 2002, **420**, 302–304.
4 P. Chen, Z. Xiong, J. Luo, J. Lin and K. L. Tan, *J. Phys. Chem. B*, 2003, **107**, 10967–10970.
5 Y. Kojima and Y. Kawai, *J. Alloy. Compd.*, 2005, **395**, 236–239.
6 Z. Xiong, G. Wu, J. Hu and P. Chen, *Adv. Mater.*, 2004, **16**, 1522–1525.
7 W. F. Luo, *J. Alloy. Compd.*, 2004, **381**, 284–287.
8 W. Luo and S. Sickafoose, *J. Alloys Compd.*, 2006, **407**, 274–281.
9 Xiong, G. Wu, J. Hu, Y. Liu, P. Chen, W. Luo and J. Wang, *Adv. Funct. Mater.*, 2007, **17**, 1137–1142.
10 L. H. Jepsen, D. B. Ravnsbæk, C. Grundlach, F. Besenbacher, J. Skibsted and T. R. Jensen, *Dalton Trans.*, 2014, **43**, 3095–3103.
11 Y. S. Chua, G. Wu, Z. Xiong and P. Chen, *J. Solid State Chem.*, 2010, **183**, 2040–2044.
12 C. Wu, Y. Bai, J. Yang, F. Wu and F. Long, *Int. J. Hydrogen Energy*, 2012, **37**, 889–893.
13 D. A. Sheppard, M. Paskevicius and C. E. Buckley, *J. Phys. Chem. C*, 2011, **115**, 8407–8413.
14 N. K. Singh, T. Kobayashi, O. Dolotko, J. W. Wiench, M. Pruski and V. K. Pecharsky, *J. Alloy. Compd.*, 2012, **513**, 324–327.
15 G. Pireddu, A. Valentoni, C. B. Minella, C. Pistidda, C. Milanese, S. Enzo, G. Mulas and S. Garroni, *Int. J. Hydrogen Energy*, 2015, **40**, 1829–1835.
16 O. Dolotko, N. Paulson and V. K. Pecharsky, *Int. J. Hydrogen Energy*, 2010, **35**, 4562–4568.
17 W. I. F. David, J. W. Makepeace, S. K. Callear, H. M. A. Hunter, J. D. Taylor, T. J. Wood and M. O. Jones, *J. Am. Chem. Soc.*, 2014, **136**, 13082–13085.
18 J. W. Makepeace, T. J. Wood, H. M. A. Hunter, M. O. Jones and W. I. F. David, *Chem. Sci.*, 2015, **6**, 3805–3815.
19 J. Guo, P. Wang, G. Wu, A. Wu, D. Hu, Z. Xiong, J. Wang, P. Yu, F. Chang, Z. Chen and P. Chen, *Angew. Chem.*, 2015, **127**, 2993–2997.
20 R. Janot, J.-B. Eymery and J.-M. Tarascon, *J. Phys. Chem. C*, 2007, **111**, 2335–2340.
21 H. Cao, T. M. M. Richter, C. Pistidda, A.-L. Chaudhary, A. Santoru, G. Gizer, R. Niewa, P. Chen, T. Klassen and M. Dornheim, *ChemSusChem*, DOI: 10.1002/cssc.201500990.
22 H. Jacobs and B. Harbrecht, *J. Less. Common Met.*, 1982, **85**, 87–95.
23 R. L. Lowton, M. O. Jones, W. I. F. David, S. R. Johnson, M. Sommariva and P. P. Edwards, *J. Mater. Chem.*, 2008, **18**, 2355–2360.
24 B. R. S. Hansen, K. T. Møller, M. Paskevicius, A.-C. Dippel, P. Walter, C. J. Webb, C. Pistidda, N. Bergemann, M. Dornheim, T. Klassen, J.-E. Jørgensen and T. R. Jensen, *J. Appl. Cryst.*, 2015, **48**, 1234–1241.
25 A. P. Hammersley, S. O. Svensson, M. Hanfland, A. N. Fitch and D. Hausermann, *High Pressure Res.*, 1996, **14**, 235–248.
26 J. Rodriguez-Carvajal, *Physica B*, 1993, **192**, 55–69.
27 M. Paskevicius, M. B. Ley, D. A. Sheppard, T. R. Jensen and C. E. Buckley, *Phys. Chem. Chem. Phys.*, 2013, **15**, 19774–19789.

28 Y. Zhong, H.-Y. Zhou, C.-H. Hu, D.-H. Wang and A. R. Oganov, *J. Phys. Chem. C*, 2012, **116**, 8387–8393.
29 H. Cao, J. Wang, Y. Chua, H. Wang, G. Wu, Z. Xiong, J. Qiu and P. Chen, *J. Phys. Chem. C*, 2014, **118**, 2344–2349.
30 B.-X. Dong, L. Song, J. Ge, Y.-L. Teng and S.-Y. Zhang, *RSC Adv.*, 2014, **4**, 10702–10707.
31 R. Černý, G. Severa, D. B. Ravnsbæk, Y. Filinchuk, V. d'Anna, H. Hagemann, D. Haase, C. M. Jensen and T. R. Jensen, *J. Phys. Chem. C*, 2010, **114**, 1357–1364.
32 H. Cao, Y. Zhang, J. Wang, Z. Xiong, G. Wu and P. Chen, *Prog. Nat. Sci.*, 2012, **22**, 550–560.
33 T. Ichikawa, N. Hanada, S. Isobe, H. Leng and H. Fujii, *J. Phys. Chem. B*, 2004, **108**, 7887–7892.

Table1 Overview of samples, synthesis procedures and products.

Name	Composition	Synthesis	Products
s1	$LiNH_2$–$NaNH_2$ (3:1)	Ball mill 5 min[(a)]	$LiNa_2(NH_2)_3$, $LiNH_2$, $NaNH_2$, $Li_3Na(NH_2)_4$[(d)]
s2	$LiNH_2$–$NaNH_2$ (3:1)	Ball mill 20 min[(a)]	$LiNa_2(NH_2)_3$, $LiNH_2$, $Li_3Na(NH_2)_4$[(d)]
s3	$LiNH_2$–$NaNH_2$ (3:1)	Ball mill 90 min[(a)]	$Li_3Na(NH_2)_4$, $LiNa_2(NH_2)_3$[(d)]
s4	s3	Annealing at 150 °C	94% $Li_3Na(NH_2)_4$, 6% $LiNa_2(NH_2)_3$
s5	$LiNH_2$–$NaNH_2$ (3:1)	Ball mill 20 h[(b)] and annealing at 150 °C	94% $Li_3Na(NH_2)_4$, 6% $LiNa_2(NH_2)_3$
s6	$Li_3Na(NH_2)_4$–LiH (1:4)	Manually grinded 5 min	$Li_3Na(NH_2)_4$ + LiH (1:4)
s7	$Li_3Na(NH_2)_4$–LiH (1:4)	Ball mill 1.5 h[(c)]	-
s8	$Li_3Na(NH_2)_4$–LiH (1:4)	Ball mill 10 h[(c)]	$LiNH_2$ + NaH + LiH (4:1:3)
s9	$LiNH_2$–LiH	Ball mill 10 h[(c)]	$LiNH_2$ + LiH (1:1)
s10	$LiNH_2$–NaH (1:1)	Ball mill 10 h[(c)]	$LiNH_2$–NaH (1:1)
s11	$NaNH_2$–LiH (1:1)	Ball mill 10 h[(c)]	$Li_3Na(NH_2)_4$ + NaH + LiH (1:3:1)
s12	$LiNH_2$	Ball mill 10 h[(c)]	$LiNH_2$

[(a)] A high energy Spex ball mill and stainless steel vials were used, [(b)]A planetary ball mill and agate vials were used, [(c)]A planetary ball mill and stainless steel vials were used. [(d)]Weak reflections observed by PXD.

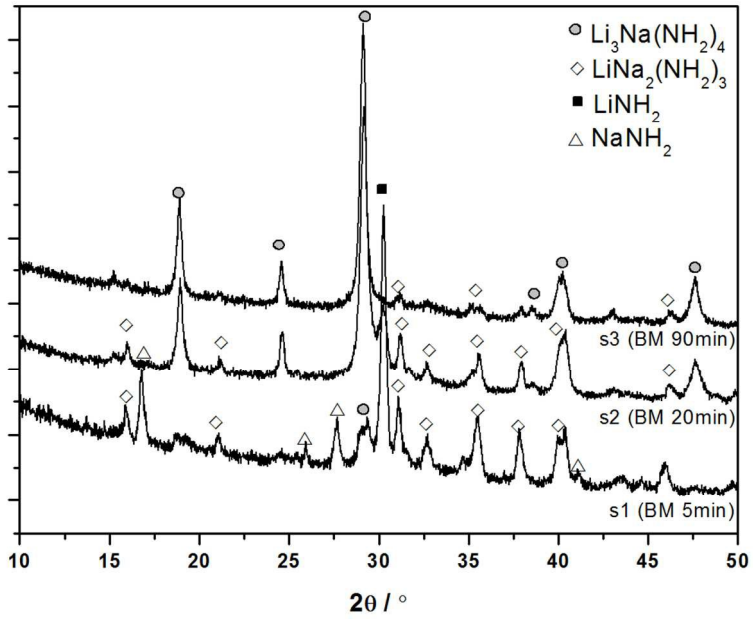

Figure 1 PXD data for $LiNH_2$-$NaNH_2$ (3:1) ball milled for 5 min (s1), 20 min (s2) and 90 min (s3) using a high energy Spex ball mill. Symbols: ■ $LiNH_2$; △ $NaNH_2$; ● $Li_3Na(NH_2)_4$; ◇ $LiNa_2(NH_2)_3$.

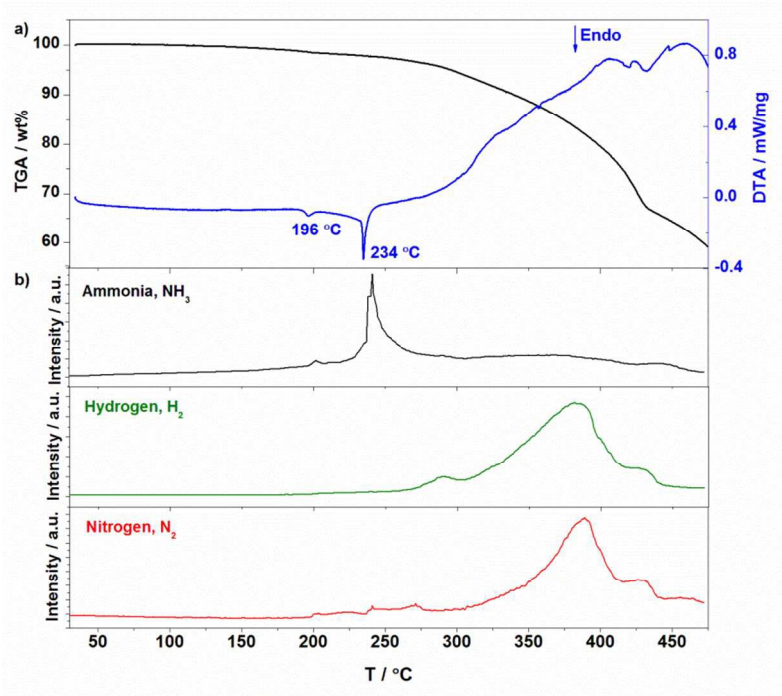

Figure 2 a) Combined TGA (black) and DTA (blue). b) TPD-MS for $Li_3Na(NH_2)_4$ (s4) during heating from RT to 475 °C at 2 °C/min.

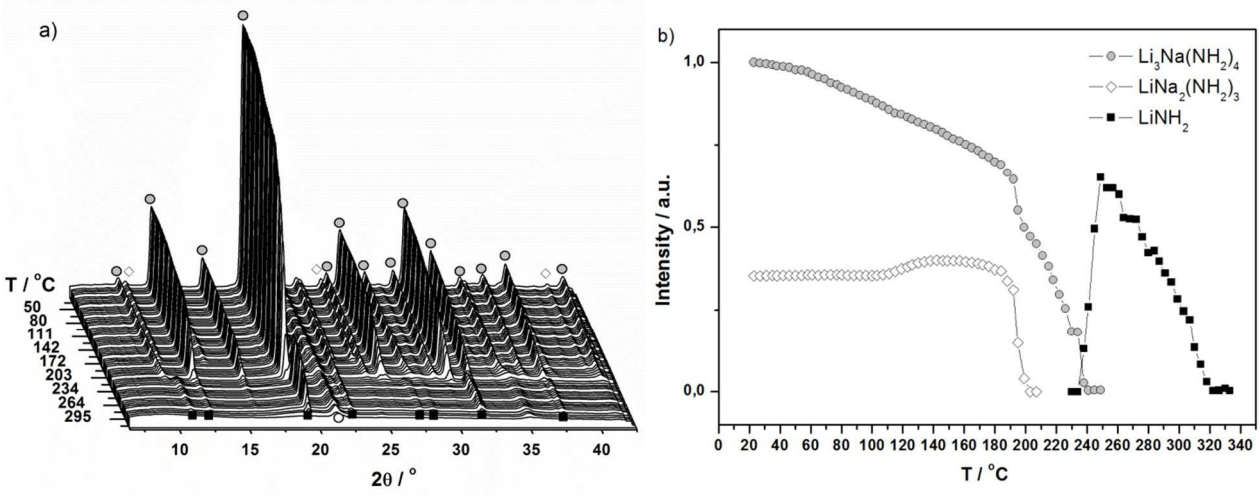

Figure 3 a) *In-situ* SR-PXD of $Li_3Na(NH_2)_4$ (s4) during heating from RT to 440 °C (5 °C/min) in argon atmosphere, λ = 0.99203 Å. b) Normalized integrated reflections plotted as a function of temperature. Symbols: ● $Li_3Na(NH_2)_4$; ◇ $LiNa_2(NH_2)_3$; ■ $LiNH_2$; ○ Li_2O

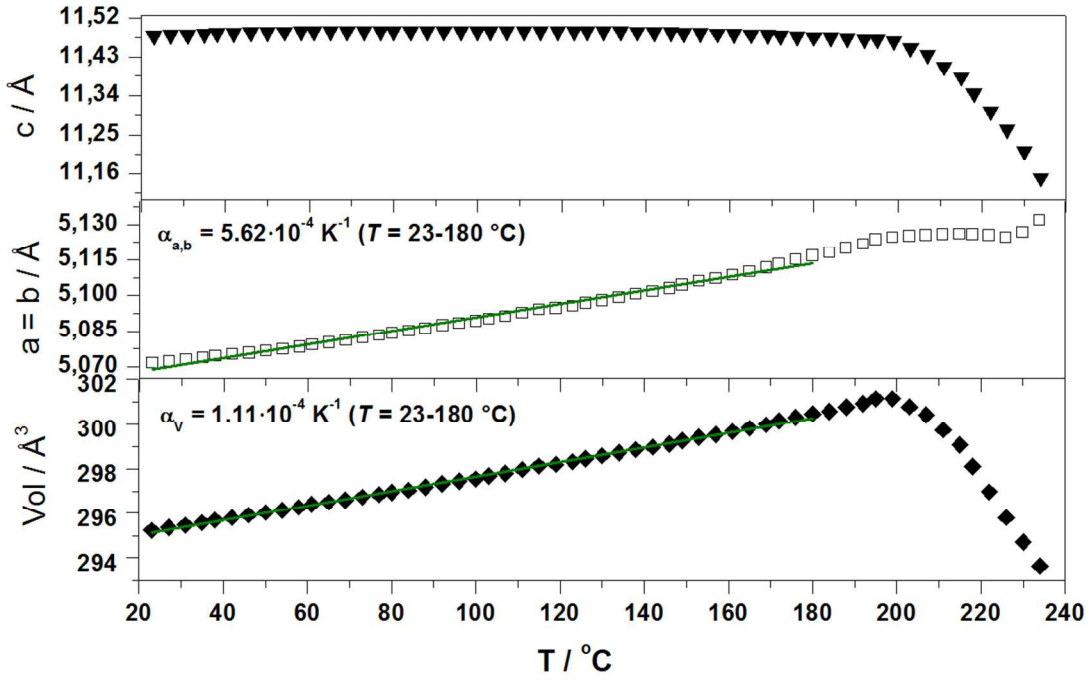

Figure 4 Unit cell parameters extracted from sequential Rietveld refinement plotted as a function of temperature for $Li_3Na(NH_2)_4$.

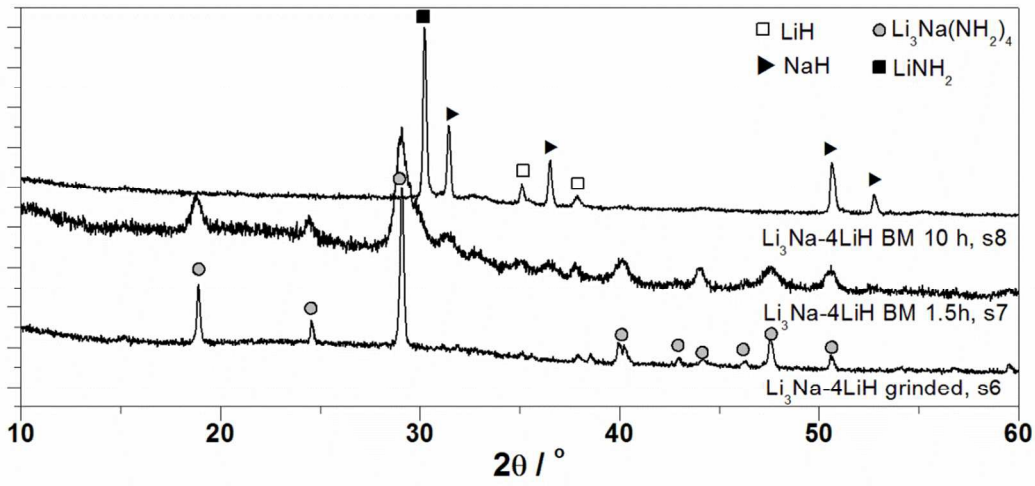

Figure 5 PXD data measured for $Li_3Na(NH_2)_4$–LiH (1:4) mixed in a mortar for 5 min (s6), ball milled for 1.5 h (s7) and ball milled for 10 h (s8), $\lambda = 1.54056$. Symbols: ○ $Li_3Na(NH_2)_4$; ■ $LiNH_2$; □ LiH; ▶ NaH.

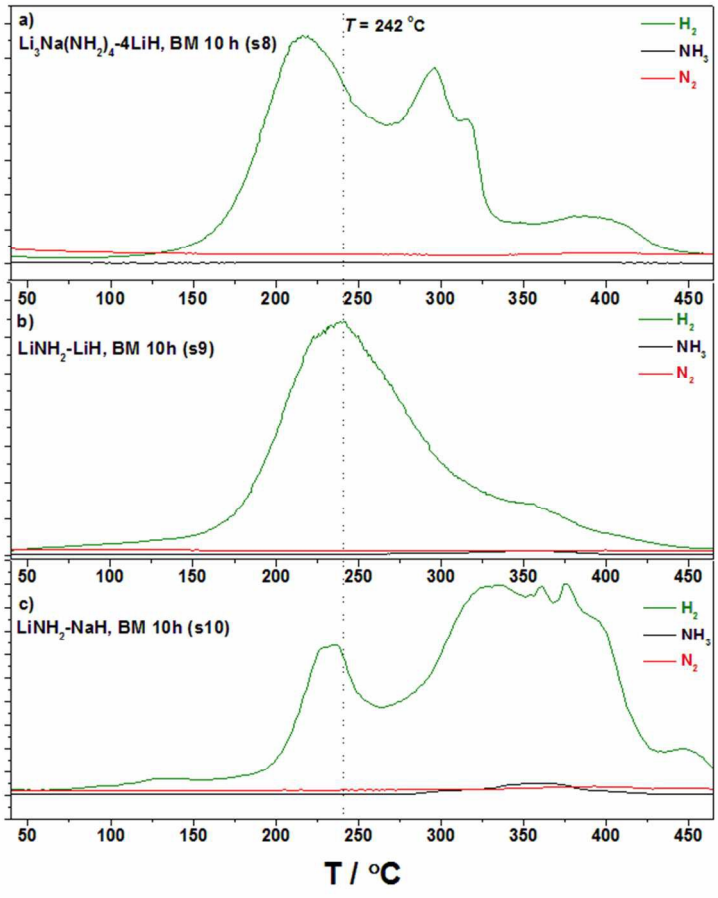

Figure 6 TPD-MS during heating from RT to 475 °C (2 °C/min) for a) $Li_3Na(NH_2)_4$–4LiH ball milled 10h (s8), b) $LiNH_2$–LiH ball milled for 10 h (s9) and c) $LiNH_2$–NaH ball milled for 10 h (s10).

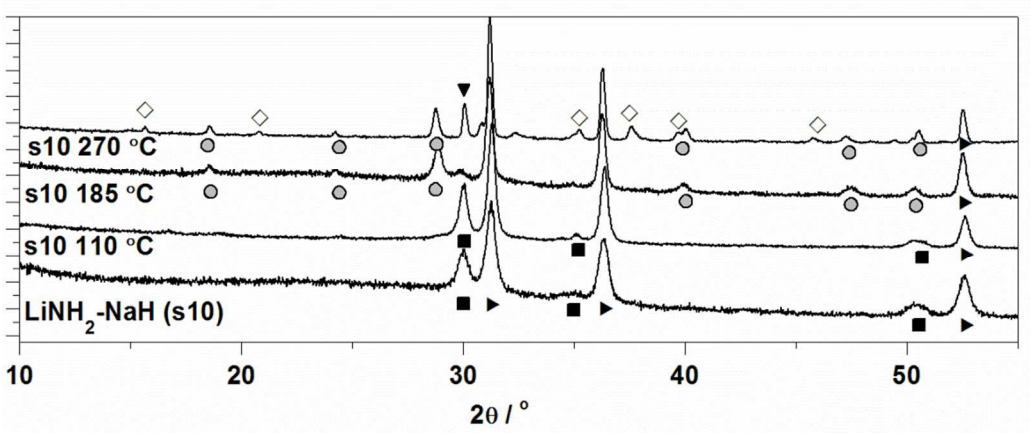

Figure 7 PXD data for $LiNH_2$–NaH (s10) and after heating s10 to 110, 185 and 270 °C, respectively. All PXD patterns were collected at RT, λ = 1.54056 Å. Symbols: ■ $LiNH_2$; ▶ NaH; ◍ $Li_3Na(NH_2)_4$; ◇ $LiNa_2(NH_2)_3$; ▼ Li_2NH.

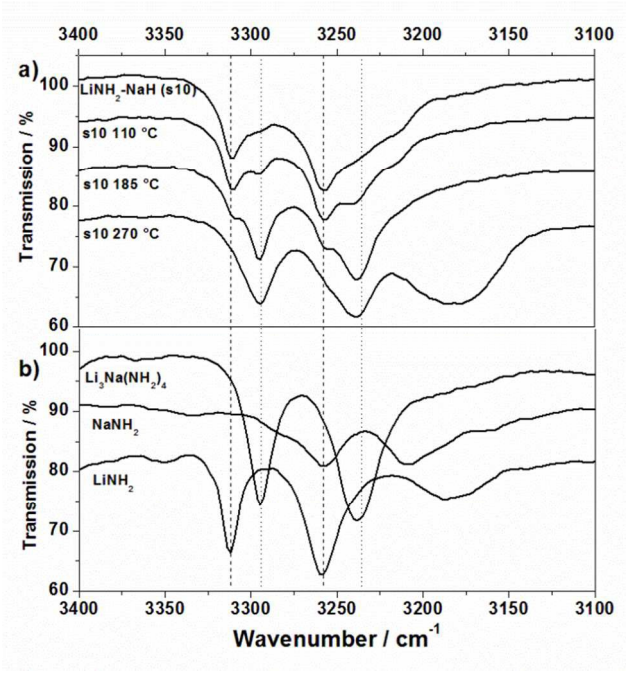

Figure 8 a) FTIR spectra for $LiNH_2$–NaH (s10) and after heating s10 to 110, 185 and 270 °C, respectively. b) Spectra for $Li_3Na(NH_2)_4$, $NaNH_2$ and $LiNH_2$ for comparison. All spectra were collected at RT.